Journal of Optoelectronics and Advanced Materials Vol. 2, No. 1, March 2000, p. 43-52

OPTICAL STUDIES OF a-C:H FILMS DEPOSITED FROM CH_4, CH_4/He, CH_4/Ar AND CH_4/N_2 rf PLASMAS

N. Tomozeiu, K. J. Clay[a], W. I. Milne[a]

Faculty of Physics, University of Bucharest, P.O. Box Mg 11,
7600 Bucharest-Magurele, Romania
[a]Engineering Department, Cambridge University, Trumpington Street, Cambridge CB2 1PZ, UK.

The deposition process of a-C:H from CH_4/He, CH_4/Ar and CH_4/N_2 rf plasmas has been studied using optical emission spectroscopy (OES). Different transitions have been identified and lines' intensities due to CH, H_α and H_β species, and the dilution gases have been monitored. The effect of the dilution gases on these species and the variation in the deposition rate of the resultant films have been discussed in terms of possible interactions within the plasma and at the film growth front. The microstructure of the resultant films, as determined from their optical properties, has been assessed as a function of the proposed growing mechanism. Further, optical properties of the resultant films, including absorption coefficient, refractive index and optical gap, have been measured and correlated with the observed OES variations.

(Received February 10, 2000; accepted March 9, 2000)

*Keywords: A*morphous carbon, PECVD, Optical emission spectroscopy, Band tail

1. Introduction

Semi-transparent amorphous hydrogenated carbon (a-C:H) films have recently attracted much attention because of their potential technological advantages. The properties promoting the interest are hardness, chemical inertness, wear resistance, bio-compatibility and infrared transparency [1,2]. In the last years, the using of the diamond like carbon (DLC) in the micro-electromechanical systems technologies [3], optically activated field effect transistors [4] and detectors for dosimetry, applications [5] is a certitude. Plasma-enhanced chemical vapour deposition (PECVD) is one of the most universally used techniques for the deposition of a-C:H because films of widely varying properties are achievable depending on the process parameters selected [6]. A potential disadvantage of this technique is, however, that the large number of process parameters involved complicates the optimisation of the deposition conditions necessary to obtain films with the desired properties.

It is well established that negative self-bias of the substrate and consequently the impacting ion energy, coupled with the ion current density, are critical in determining the film properties [7]. However, it was found that the gas phase composition of the rf plasma also plays a key role in determining the nature of the resulting film [8]. Knowledge of the relationship between plasma diagnostic measurements and the optical properties of the associated films will be useful in the optimisation of their performance. In this paper we have investigated, using optical emission spectroscopy (OES), the composition of a number of plasmas used for the deposition of a-C:H films. We have also studied, the modifications in the films' optical absorption properties brought about by varying the substrate bias and the gas composition, i.e. by inclusion of He, Ar or N_2 into the CH_4 plasma. We have attempted to explain these variations in terms of changes in the plasma chemistry and fractionation efficiency and in the subsequent growth processes of the resultant films.

2. Experimental details

The a-C:H films were deposited from CH_4 and mixtures of CH_4 with He, Ar or N_2 onto Si-crystalline (100) and glass substrates using a rf-PECVD system. The rf plasmas were generated from a 13.56 MHz rf power supply being applied between two capacitively coupled parallel plate electrodes. Prior to being placed in the reactor chamber, the substrates were cleaned in an ultrasonic bath with methanol, acetone and isopropyl alcohol after a nitric acid dip. The substrate was further treated with an in-situ Ar sputter clean prior to deposition.

The lower powered electrode, on which the substrates were placed, was maintained at 20° C by a feedback controlled cooling system. The gas flow rates were 5 sccm/45 sccm for CH_4-Ar and CH_4-He and 5 sccm/0.5 sccm for CH_4-N_2. Films were grown at a fixed pressure (100 mTorr) but with different rf powers (i.e. 30 W, 120 W and 210 W). This produced different negative dc bias voltages, which were measured using a dc voltmeter (via a matching network), and substrate temperatures, which were measured during deposition. We used temperature micro-dots that are dried liquids that change colour at certain temperature. They were shielded from, but in close proximity to the plasma.

Optical emission spectroscopy (OES) of the plasma discharge was performed in the range 300 - 900 nm, through an optical fibre fixed on a quartz window mounted in the chamber-reactor wall, on which the collected light was focused.

Ellipsometry, at a wavelength of 632.8 nm, was used to determine thickness and refractive index of deposited films on the silicon substrates. Thickness was also checked by profilometric measurements. Using a stylus profilometer (Dektak 3030), we have measured the height of a step produced by masking the sample during the deposition. Normal incidence optical transmission and reflection measurements were performed on the glass substrates, using a dual beam ultraviolet-visible (UV-VIS) spectrometer in the range 400 nm – 900 nm. The optical band-gap of the deposited a-C:H films was determined from absorption coefficient spectra. We have used two definitions of this optical parameter: E_{04}, which is the photon energy at which the absorption coefficient is equal to 10^4 cm^{-1} and E_{gT}, which is obtained from the Tauc plots.

3. Results

3.1. Optical emission spectroscopy

Typical emission spectra of rf plasmas from CH_4 and CH_4-He, CH_4-Ar and CH_4-N_2 mixtures are shown in Figs. 1a, 1b, 1c and 1d, respectively. The most intense lines in the CH_4 spectrum (Fig. 1a) are due to the emissions from CH radicals (390 nm and 430 nm), atomic hydrogen (H_α at 656 nm, H_β at 486 nm and H_γ at 434 nm), and molecular hydrogen (H_2 bands centred at 463 nm and 602 nm) [9].

The emission spectra from the mixed plasmas (CH_4-He [Fig. 1b], CH_4-Ar [Fig. 1c], and CH_4-N_2 [Fig. 1d]) are a combination of the transitions of a CH_4 plasma discharge and Ar, He lines or N_2 bands. As is shown in Figs. 1b – 1d, the additive gas transitions are the most significant in the emission spectra. We have to point out that the geometry of the OES measurement system and the conditions of the data acquisition were conserved during all measurements.

The OES spectrum of the CH_4-He plasma (Fig. 1b) shows a system of peaks due to atomic and ionic He transitions [10]. The strongest of these are placed at 389, 447, 502, 588, 668 and 706 nm. For the CH_4-Ar plasma, the OES spectrum (Fig. 1c) shows a system of peaks that can be assigned to the atomic lines of Ar. Thus, most part of them are placed in the 700 -850 nm region (the most intense lines being at 751 and 811 nm) and form so-called Ar I group. There are also some weak peaks that can be ascribed to Ar II lines – group, in the 415 - 490 nm region.

The optical emission spectrum of the CH_4-N_2 plasma (Fig. 1d) shows peaks centred at 316, 337, 380, 400 and 420 nm, which correspond to vibration/rotation bands due to the second positive molecular bands of N_2. Lines at 391 and 428 nm are due to the first negative system of N_2^+, while peaks centred at 540, 580, 650 and 750 nm are associated with the first positive system of the N_2. A

band head at 388 nm is due to CN molecules that are produced by reactions between excited molecules of CH_x and N_2.

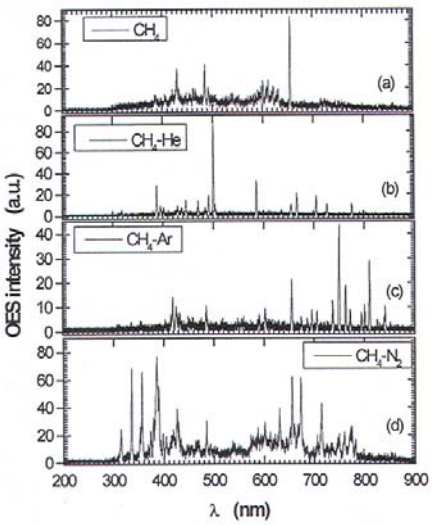

Fig. 1. Typical optical emission spectrum from (a) CH_4, (b) CH_4-He, (c) CH_4-Ar, and (d) CH_4-N_2 rf PECVD plasmas.

The variation, with rf power, in the emission intensity for the CH (430 nm) line and the H_α (656 nm) line, for the different mixed CH_4/diluent plasmas studied, are shown in Figs. 2a and 2b, respectively. It can be seen (Fig. 2a) that the CH band shows an almost linear increase with power regardless of the plasma mixture. In the case of the H line (Fig. 2b), the intensity increases for all mixtures above a threshold power density of about 60 W. However, relative to the pure CH_4 plasma, Ar promotes the increase, He reduces it, while N_2 has no effect. We have to point out that the nitrogen amount used is not comparable with Ar or He.

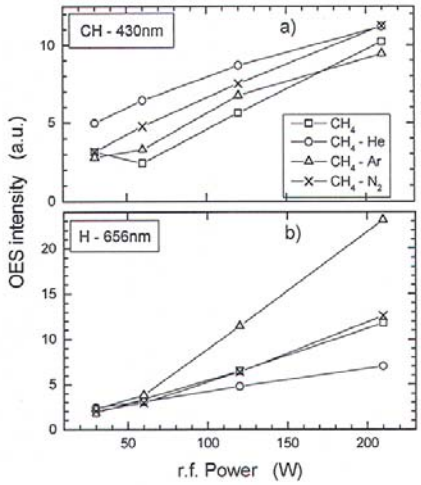

Fig. 2. Variation of optical emission intensities of (a) CH [430nm] and (b) H_α [656nm] with plasma mix (CH_4, CH_4-He, CH_4-Ar, or CH_4-N_2) as a function of rf power.

Further, from the mixed CH_4 with He or Ar plasmas we have monitored He and Ar atomic line intensities (389 and 501 nm for He; 419 and 750 nm for Ar) as a function of power (Fig. 3a). We have observed that all lines increase in intensity, with rf power. For the CH_4-N_2 plasma, the line intensities [N_2 2nd positive (358 nm), CN (388 nm), N_2^+ (391 nm) and N_2 1st positive (661 nm)] were also monitored with power and these are plotted in the Fig. 3b. There is an increase in the intensities of all species, but those for N_2 and CN are largest.

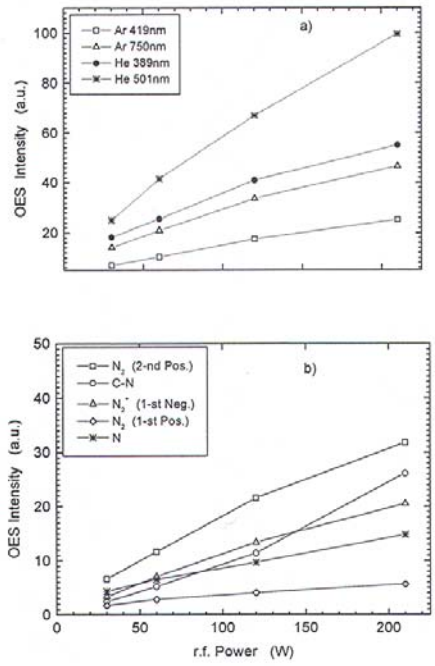

Fig. 3. Variation of optical emission intensities of (a) Ar and He species from CH_4-He, CH_4-Ar plasmas and (b) nitrogen species from CH_4-N_2 plasmas as a function of rf power.

3.2. Growth of deposited films

The deposition rates of the a-C:H films deposited from CH_4 and the various binary CH_4/gas mixtures, as a function of rf power, are shown in Fig. 4. It can be seen that increasing rf power values, the deposition rates of films grown from CH_4/He plasmas, although lower, follow the same trend as those deposited from pure CH_4 plasmas. With Ar dilution of the CH_4 or N_2 addition, the deposition rate trends are quite different. At low rf power, N_2 has little effect on the deposition rate but there is a significant linear reduction with the increasing rf power. With Ar dilution, at low rf power, the deposition rate tracks that of the He dilution but increasing power (and the dc bias voltage) the deposition rate falls off to the level observed for the N_2 diluted films. These differences will be explained in section 4 using the competition between etching and deposition mechanisms.

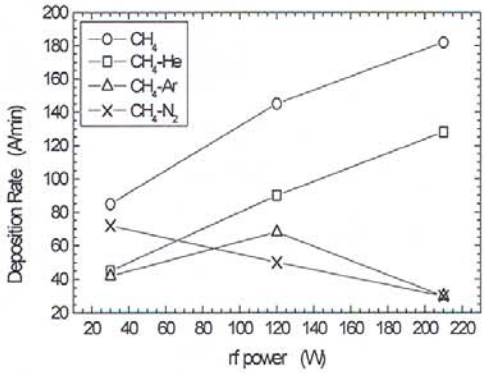

Fig. 4. Deposition rate as function of rf power for a-C:H films deposited from CH_4 (-o-), CH_4-He (-□-), CH_4-Ar (-Δ-), and CH_4-N_2 (-x-) rf PECVD plasmas.

3.3. Optical properties

Measurements of optical transmission and reflection were made on each carbon specimen in the range 1.4 - 3.2 eV, from which the optical absorption was determined using the $A=1-T-R$ relationship, where R is the reflectivity and T is the transmission. For comparison, the optical absorption coefficient, α, for samples deposited at 210 W from CH_4-He, CH_4-Ar and CH_4-N_2, are plotted in Fig. 5a.

The influence of the rf power on the $\alpha(E)$ spectrum is shown in Fig. 5b for samples deposited from CH_4-He plasmas. The larger the rf power, the larger is the absorption coefficient value. This trend was observed for all the binary gas-mixtures used during deposition.

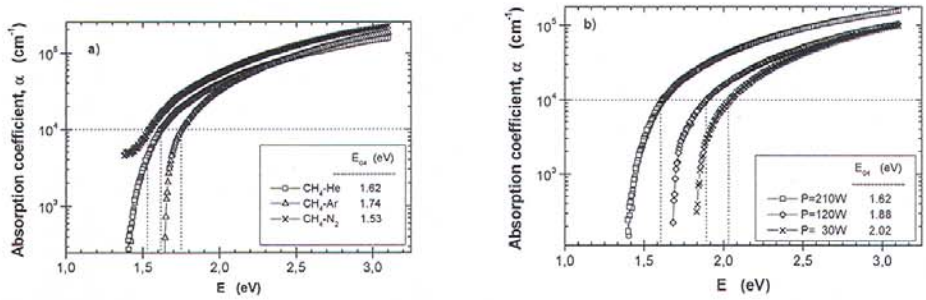

Fig. 5. Optical absorption coefficient spectra and E_{04} band gap values for: (a) plasma mix (CH_4-He, CH_4-Ar, and CH_4-N_2) at fixed rf power (210 W) and (b) power, at fixed plasma mix (CH_4-He).

The optical gap defined as E_{04}, can be determined from the plot plot in the semilogarithmic scale. Thus, samples deposited from CH_4-He plasmas are characterised by an optical gap smaller than the gap of those deposited from CH_4-Ar plasmas. For example at 210 W rf power, the E_{04}= 1.62 eV for sample deposited in the presence of He and E_{04}= 1.74 eV, when is used Ar for dilution. Varying the rf power, in the CH_4-He plasmas case, the smaller is the rf power, the larger the optical gap: E_{04}= 1.62 eV for sample deposited with 210 W and E_{04}= 2.02 eV when 30 W were used. These are explained by the changing of structure with both, the gas used for dilution and the rf power.

Using the Tauc-plots, the optical band gap of the films was determined, in accordance with the expression [11]:

$$\sqrt{\alpha E} = B\left(E_{gT} - E\right) \tag{1}$$

where E is the photon energy and B is an empirical constant. The Tauc gap (E_{gT}) was obtained from the intercept of the extrapolated linear part of the curves with the energy axis. The E_{gT} values as a function of diluent type and rf power are shown in Figs. 6a and 6b, respectively.

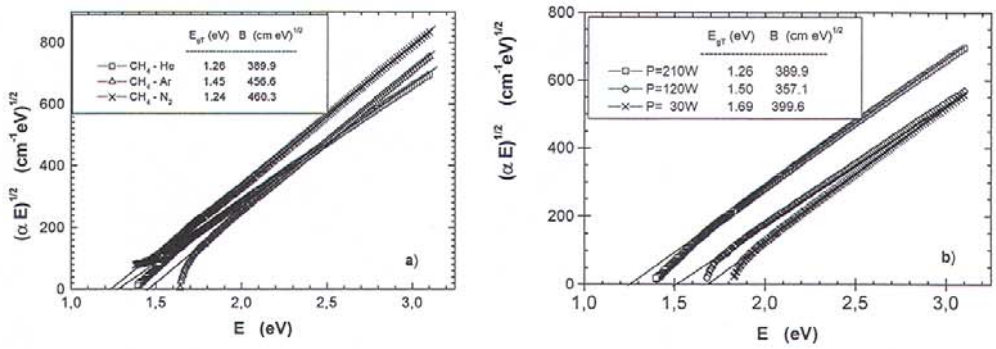

Fig. 6. Variation in the Tauc slope (B) and optical band gap (E_{gT}) with: (a) plasma mix (CH_4-He, CH_4-Ar, and CH_4-N_2) at fixed rf power (210 W) and (b) power, at fixed plasma mix (CH_4-He).

4. Discussions

4.1. OES analysis

The intensity of a plasma optical emission due to a species with the concentration given by *[X]* may be expressed by:

$$I_x = C_x(E)\ \eta_x\ [X] \tag{2}$$

where the rate coefficient $C_x(E)$ is a function of the energy of the electrons. This is dependent upon the plasma sheath electric-field-to-pressure ratio F/p, which is directly proportional to the self-bias voltage, V_b. The excitation efficiency η_x is a function of the density and energy distribution of the electrons.

The increase in the intensities of all optical emission bands with rf power (Figs. 2 and 3) is due to an increase in electron temperature, T_e, and density (and therefore C_x) with bias voltage, resulting in an increase of all reaction processes which are taken place in plasma volume, [12].

The higher relative intensities of the OES active plasma species derived from the diluent gases in comparison with those for the species derived from CH_4 (Fig. 1) can also be explained by referring to Eq. (2). With He and Ar, there is a contribution from *[X]* due to their higher concentration (45 sccm) relative to CH_4 (5 sccm). This, however, does not fully explain the increased intensities. This is highlighted by the inclusion of N_2 with a lower concentration (0.5 sccm). The rate coefficient $C_x(E)$ is constant therefore the increased intensities must be due to higher excitation efficiencies, η_x, of the diluent gases relative to CH_4. The increased slopes of the intensities of different species (e.g. He [501 nm], N_2^+ and CN [Fig. 3]) may reflect higher activation energies or multiple activation pathways for the generation of these species.

In the case of the H_α (656 nm), the intensity variation with the addition of Ar and He (Fig. 2b) must be due to a change in the concentration *[X]* of H_α since the rate coefficient and

activation energy are constant. In fact, it is known that atoms of the dilution gases realise a physical sputtering of the film surface. The Ar sputter bombardment results in a film with a lower hydrogen content [12]. This could be explained by sputter yielding of hydrogen due to the surface bombardment of both, Ar atoms and complex C_xH_y molecules, at the growth surface. In such a way we see the much steeper increase (Fig. 2b) of the H_α optical emission when Ar is used.

In a He-CH_4 plasma, excited He (2^3S), He (2^1S) and He^+ ($2S$) species are generated, which have reaction rate coefficients with CH_4 molecules of 2, 4 and 13×10^{-10} cm^3s^{-1}, respectively, [14]. These species can effect additional CH_n^+ ion generation through Penning ionisation and dissociation. In particular, with an excitation energy of 19.8 eV (5 eV below the ionisation potential of He), the He (2^3S) atoms can play a major role in producing CH_4^+ and CH_3^+ ions. In the CH_4-He plasmas the He^+ and/or the hydrocarbon ions contribute to the maintenance of the plasma. The ionisation potential of He (24.5 eV) is much higher than the threshold potentials for the generation of CH_4^+ and CH_3^+ ions from CH_4 molecules (12.6 eV and 14.3 eV, respectively), [14], thus at low rf power, Penning ionisation will not be significant. Increasing the rf power (and from here, the sheath electric field), the increased densities of these metastable He atoms lead to an increase of the CH_4^+ and CH_3^+ ions density over and above that which is expected due to the increase in T_e. This, in turn, alters the balance of the CH_4 fractionation reactions due to collision and capture cross-section changes and may account for the increased CH emission and reduced H intensities observed in the CH_4-He plasmas relative to CH_4 (Fig. 3). The densities of the ions $C_2H_5^+$ and CH_5^+, generated from secondary reactions, have been shown to be maximised at a critical CH_4 composition in He close to that used in this study and to promote film formation [14].

The effect of nitrogen inclusion on the film growth from the CH_4/ N_2 plasma was discussed in a previous paper, [15]. The deposition data (Fig 4) presented here, confirm our conclusion that the decrease in film growth rate with increasing rf power is due to an increase in the ion bombardment energy and density of N_2^+. This species acts as an efficient chemical/physical sputter agent despite the low concentration of N_2 (N_2/ CH_4 >10%). Etch rate measurements show [8] that the sputter yield from N_2 increases from 2 to 3 orders of magnitude above that of Ar over the power range studied. Further, nitrogen inclusion in the film leads to an a-C:H(N) structure.

4.2. Optical properties

Amorphous carbon can have three local configurations and, therefore, three band structure: a) sp^3 configurations for which σ and σ^* bands exist; b) sp^2 and c) sp^1 configurations for which both types σ and π bands exist with their corresponding σ^* and π^* bands. There have been reported, [16], of minor amounts of sp^1 bonding in a-C:H films but generally, the microstructure is discussed in terms of sp^3 / sp^2 ratio and H content with maximised sp^3 / sp^2 ratio and reduced H content considered necessary for the most desirable diamond-like (DLC) films [17]. Optical properties are particularly sensitive to the microstructure as they are related to the electronic band structure [18,19].

The deposition mechanism of a-C:H films in a CH_4 rf plasma involves the diffusion of CH_n (predominantly CH_3) radicals onto the substrate surface and ion bombardment which create dangling bonds (defect sites) by sputtering of bonded hydrogen atoms. Further hydrocarbon species or hydrogen are then adsorbed at these active sites. At low rf power, low energy ion bombardment leads to limited surface bond breakage resulting in a soft polymer-like carbon film. With increasing ion energy, carbon network break-up is promoted, with sufficient energy to facilitate local densification leading to formation and stabilisation of sp^3 CH_2 bonding found in diamond-like carbon films. Further increases in ion energy, however, result in excess energy dissipation and relaxation of the network leading to increased formation of sp^2 CH π bonding and graphite-like carbon [17,18].

It is known that for amorphous semiconductors the states from the tail state band are due to the disorder while the localised states close to the Fermi level have their origin in defect sites. The width of the tail band is, therefore, a measure of the disorder in a material. Using the Tauc theory to determine the optical gap, the slope B of the Tauc plot is inversely proportional to the square root of the width of the tail state band [20].

Our results show (Fig. 6b) that although the band gap decreases with power, slope B initially decreases (30 – 120 W) and then increases (120 - 210 W). Polymeric rf deposited a-C:H films are predominantly sp^3 CH_3 in nature with high H content and a high optical band gap. The sp^3 CH_3 and sp^3 CH_2 components are indistinguishable thus it is not surprising that the band gap decreases with rf power increase. The slope B variation, however, reflects the polymer-like, diamond-like and graphite-like film progression, when the rf power is increased.

The optical band gap for films deposited from gas mixtures (Fig. 5a and 6a) decreases in the order Ar > He > N_2. Our measurements of slope B (Fig. 6a) show, however, that the band tail becomes progressively wider for samples deposited from He, Ar and N_2 plasmas. These results confirm that the total mix of the various forms of sp^3 and sp^2 and their medium-range order will dictate the true microstructure of the films.

The sputter etch of hydrogen creates dangling bonds and plays a key role in the formation of sp^3CH bonding in DLC films [21]. The fact that Ar ion bombardment increases the sputter etch of hydrogen [13] is confirmed by the increased OES emission of H lines with the inclusion of Ar (Fig. 2b). Since the polymeric component and H content are reduced, the higher band gap of Ar deposited films may reflect increased amounts of sp^3CH. Increased defect site generation and Ar inclusion in interstitial lattice sites may, however, account for the increased width of the tail state band.

With the inclusion of He, the increased flux of C_xH_y ions will result in increased dangling bond creation but the higher densities of H and C_xH_y species at the film growth front will lead to increased active site passivation resulting in a more densely packed carbon network with fewer defect sites and a reduced width of the tail state bands. The reduced hydrogen emission intensity (Fig. 2b) with He inclusion may reflect increased H combination with C_xH_y species at the growth front.

In the case of CH_4-N_2, the N_2^+ ion acts as an efficient chemical/physical sputter agent. Thus dangling bond generation is increased. The development of the CN band in the OES spectra (Fig. 3) suggests that active C_xN_y species are generated either in the plasma or at the growth front. Passivation of active sites by these species introduces complex nitrogen bonding which leads to a different a:C-H:N film structure with an increase in the sp^2 bonding.

A more rigorous analysis of optical properties may allow a further elucidation of the true microstructure of these films. Conventionally a gaussian distribution of the π -type states in the tail of the allowed band is assumed. If this is written for the valence band tail as:

$$N(E) = \frac{N_V}{\sqrt{2\pi}} \exp\left[-\left(\frac{E - E_V}{\delta\sqrt{2}}\right)^2\right] \tag{3}$$

where N_v is the density of states at the valence band edge, E_v and δ is the standard deviation, the value of N_v can be estimated from absorption values. Thus, for photons with energy equal to the optical gap, all the electrons from the tail of the valence band are excited into the conduction band:

$$N_T = \int_{E_V}^{E_V + E_W} N(E)dE = \frac{\delta N_V}{2} erf\left(\frac{E_w}{\delta\sqrt{2}}\right) \tag{4}$$

where N_T is the total number of electrons from the localised states in the valence band tail, E_w is the width of valence band tail, and erf(x) is the error function.

Assuming that all localised states from the tail are absorption centers, the absorption coefficient is given by [22]:

$$\alpha = \frac{\pi e^2 f}{nm} N_T \tag{5}$$

where e is the electron charge, f is the oscillator strength (which is of the order of unity), m is the electron mass and n is the refractive index of the sample.

Introducing equation (4) into expression (5) for the absorption coefficient, gives:

$$N_v = \frac{2m}{\pi e^2 f} \cdot \frac{n\alpha}{\delta \, erf\left(\frac{E_w}{\sigma\sqrt{2}}\right)} \tag{6}$$

Assuming for the width of the band tail a value $E_w = \delta\sqrt{2}$, the relative value of the density of states at the valence band edge can be estimate from relationship (6). Thus, assuming that the Tauc plot slope is related to the width of the band tail, as:

$$\sqrt{B} = \frac{4\pi\sigma_{min}}{ncE_w} \propto \frac{1}{E_w} \propto \frac{1}{\delta} \tag{7}$$

the value of N_v for one sample relative to another can then be calculated.

As an example, in the case of the CH_4-He deposited films, taking the 210 W deposited film as reference, the ratio is given by:

$$\frac{N_V(i)}{N_V(He-210)} = \frac{n(i)}{n(He-210)} \sqrt{\frac{B(i)}{B(He-210)}} \tag{8}$$

where B(i) and B(He-210) represent the Tauc plot slope for sample "i" and for sample deposited with He at r.f. power = 210 W, respectively. N_v is the density of localized states in the valence-band tail and n is the refractive index. Both these amounts, are defined for sample "i" and for the "reference" sample (deposited with He for 210 W).

For films deposited at 120 W, the ratio is 0.805 while for those deposited at 30 W the value is 0.853. These results are in good agreement with the fact that the films deposited from CH_4-He plasma at 120 W rf power are more diamond-like: small amount of density of states and narrow band tail. Recently, Maharizi et al. [23] have shown that, for the optimum conditions of deposition, the diamond bond concentration in a-DLC films prepared by rf plasma glow discharge in CH_4 remains constant up to a given thickness of the film, then decreases. The relation outlined above could be a valuable tool for experimentalist to characterise the obtained film properties relatively at one which is taken as reference. To be able to determine the absolute value of the density of states at the valence band edge, however, the electrical conduction mechanisms within the tail states would need to be assessed.

5. Conclusions

The optical properties of carbon films produced by rf plasma decomposition of methane depend strongly on the type and energy of ions within the plasma. We have studied:

i) the plasma quality as a function of gases used to enhance it;

ii) the optical properties if deposited layers.

The results can be summarised as follows:

a) emission peaks due to CH, H and H_2 were observed in CH_4-He, CH_4-Ar and CH_4-N_2 plasmas;

b) in the CH_4-He plasma, the CH_n^+ ions generated by electron collisions with CH_4 molecules have a great contribution to film growth;

c) in the CH_4-N_2 plasma CN groups are found and they modify the film quality;

d) the deposition rate is higher for CH_4-He plasmas (71.6 Å/min) and smaller for CH_4-N_2 plasmas (39.4 Å /min) and depends on rf power;

e) for films deposited from CH_4-gas mixture, the optical band gap decreases in the order Ar > He > N_2 whereas the band tail – a measure of disorder – becomes wider in order He < Ar < N_2.

f) the optical band gap (Tauc gap) decreases from 2.02 eV to 1.60 eV when the rf power increases from 30 W to 210 W;

References

[1] H. Tsai, D. B. Bogy, J. Vac. Sci. Technol., **A5**, 3287 (1987).
[2] J. C. Angus, C. C. Hayman, Science, **241**, 877 (1988).
[3] E. Kohn, P. Gluche, M. A. Adamschiik, Diamond and Rel. Mat., 8, 934 (1999).
[4] S. P. Lansley, H. J. Looi, M. D. Witfield, R. B. Jackman, Diamond and Rel. Mat., 8, 946 (1999).
[5] P. Bergonzo, F. Foulon, R. D. Marshall, C. Jany, A. Brambilla, R. D. McKeag, R. B. Jackman, Diamond and Rel. Mat., 8, 952 (1999).
[6] G. A. J. Amaratunga, S. R. P. Silva, D. R. McKenzie, J. Appl. Phys., **70**, 5374 (1991).
[7] A. D. Huypers, H. J. Hopman, J. Appl. Phys., **67**, 1229 (1990).
[8] K. J. Clay, S. P.Speakman, N. Morrison, N. Tomozeiu, W. I. Milne, Diamond and Related Materials, **7**, 1100 (1998).
[9] C. Barholm-Hansen, M. D. Bentzon, J. B. Hansen, Diamond and Related Materials, **3**, 564 (1994).
[10] E. de la Cal, D. Tafalla, F. L. Tabares, J. Appl. Phys., **73**, 948 (1993).
[11] N. F. Mott, E. A. Davis, Electronic Processes in Non-Crystalline Materials, (Clarendon, Oxford, 1971).
[12] T. DebRoy, S. Kumar, K. Tankala, Diamond and Related Materials, **4**, 69 (1994).
[13] L. H. Chou, W. T. Hsieh, J. Appl. Phys., **75**, 2257 (1994).
[14] N. Mutsukura, K. Miyatani, Diamond and Related Materials, **4**, 342 (1995).
[15] K. J. Clay, S. P. Speakman, G. A. J. Amaratunga, S. R. P. Silva, J. Appl. Phys., **79**, 7227 (1996).
[16] Y. Catherine, Mater. Sci. Forum, **52 & 53**, 175 (1989).
[17] H. J. Lee, R. Zubeck, D. Hollars, J. K. Lee, M. Smallen, A. Chao, J. Vac. Sci. Technol., **A11**, 3007 (1993).
[18] J. Robertson, Surf. Coat. Technol., **50**, 185 (1992).
[19] Y. Lifshitz, Diamond and Related Materials, **3-5**, 388 (1996).
[20] A. Madan, M.P. Shaw, The Physics and Applications of Amorphous Semiconductors, Academic Press Inc., (1988) p. 45.
[21] N. Mutsukura, S. Inoue, Y. Machi, J. Appl. Phys., **72**, 43 (1991).
[22] H. Y. Fan, Rep. Prog. Phys., **19**, 107 (1955).
[23] M. Maharizi, D. Peleg, D. Seidman, N. Croitoru, J. Optoel. Adv. Mat., **1**(4), 65 (1999).